

# AUTOMATED DETECTION AND GRADING OF HARD EXUDATES FROM RETINAL FUNDUS IMAGES

Hussain F. Jaafar, Asoke K. Nandi and Waleed Al-Nuaimy

Department of Electrical Engineering and Electronics  
The University of Liverpool, Brownlow Hill, Liverpool, L69 3GJ, UK  
Email: {h.jaafar, a.nandi, wax} @liverpool.ac.uk, web: www.liv.ac.uk

## ABSTRACT

Diabetic retinopathy is the major cause of blindness and the appearance of hard exudates is one of its earliest signs. In this study, an automated algorithm to detect and grade the severity of hard exudates is proposed. The detection process is based on top-down image segmentation and local thresholding by a combination of edge detection and region growing. Using features of the fovea and their geometric relations with other retinal structures, a method for the fovea localisation is proposed. Grading of hard exudates was performed using a polar coordinate system centred at the fovea. The results of hard exudate detection process were validated based on clinician hand-labelled data (ground truth) with an overall sensitivity of 93.2%. The superior performance of this technique suggests that it could be used for a computer-aided mass screening of retinal diseases.

**Index Terms**— Medical imaging, retinal image, hard exudate detection, top-down image segmentation.

## 1. INTRODUCTION

Diabetic retinopathy (DR) is an eye disease that is associated with long-standing diabetes and is the major cause of poor vision. Earliest signs of DR are damage to the tiny blood vessels and then the formation of lesions such as hard exudates (HEs) which are lipid leaks from the blood vessels [1]. If the disease is detected in the early stages, treatment can slow down the progression. However, this is not easy task, as DR often has no early warning signs.

Colour fundus images are used to extract features and detect HEs in retinas as well as to establish their locations, sizes, and the severity grade. Fig. 1 shows a typical fundus image with its main features and HEs. Detection and grading of DR in the fundus image are very important to assist clinicians for early diagnosis of eye diseases and then taking timely the right decision for the appropriate treatment.

HEs are normally detected and graded manually from fundus photographs by clinicians in a time-consuming and laborious intensive process. Hence, computer-aided HEs detection and grading could offer immediate and precise diagnosis to specialist inspection. Consequently, automatic detection of HEs from retinal fundus images is clinically significant.

Many different studies to detect HEs can be found in the literature. In Osareh *et al.* [2] the colour retinal image is segmented using fuzzy C-means clustering followed by

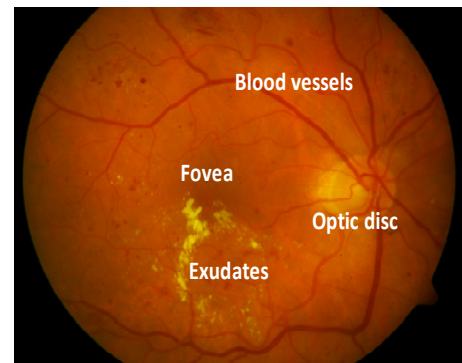


Fig. 1 – Colour fundus image with retinal structures and HEs.

classifying the segmented regions into exudates and non-exudates by an artificial neural network classifier with a sensitivity of 93.0%. In Garcia *et al.* [3] a combination of local and global thresholding was used to segment exudates followed by investigating three neural network classifiers to classify exudates with a sensitivity of 87.6%. Sanchez *et al.* [4] proposed an algorithm based on mixture models to separate exudates from the background with a sensitivity of 90.2%. Sopharak *et al.* [5] carried out series of experiments on a feature selection followed by exudates classification using naive Bayes and support vector machine classifiers and achieved a sensitivity of 92.3%. Walter *et al.* [6] proposed a method to detect exudates using their high gray level variation to determine their contour by means of morphological reconstruction techniques and got a sensitivity of 92.8%.

In this work, an automated scheme for detecting and grading HEs is proposed. The success of our technique is attributed to the utilisation of top-down image segmentation in which the image is partitioned into homogeneous sub-images as important preliminary step for accurate HE detection. With respect to grading exudates, a fovea coordinate system is adopted based on a method proposed in a previous work. Details of the proposed methods are presented in Section 2. Results and discussions are presented in Section 3, while Section 4 consists of our conclusions and future work.

## 2. METHODOLOGY

The proposed method is designed to detect and grade HEs from the retinal fundus image automatically. It consists of four main steps: image pre-processing, localisation of the fovea, HEs detection and presenting an existing system for grading the severity of HEs with additional description.

## 2.1 Pre-processing

Retinal features and HEs appear more contrasted in the green channel component than those in the other channels of the colour image [6]. Hence, in this paper the green channel component is used in the fovea localisation and HEs detection. The green channel image, shown in Fig. 2(a), was smoothed using two filtering stages; first by a median filter with a window size of  $3 \times 3$  and then by a Gaussian filter with  $\sigma = 2$ . The shade correction was carried out using morphological operations. The background intensity is estimated by applying morphological alternating opening and closing with the appropriate structuring element to be large enough to avoid entirely fitting within small candidate regions. The shade corrected image was generated by subtracting this estimated background from the smoothed image.

A process of contrast enhancement is vital to improve the contrast of image features and HEs from the background. For this, a Contrast-Limited Adaptive Histogram Equalization (CLAHE) was applied to the result of the shade correction. CLAHE enhances the image by transforming the intensity values of the image. It operates on small regions instead of the entire image. The contrast of each small region is enhanced with histogram equalization. After the equalizations, the neighboring small regions are combined using bilinear interpolation. The pre-processed image is shown in Fig. 2(b).

## 2.2 Fovea Localisation

The fovea is the part of the eye that is responsible for central vision which is necessary for all activities when visual detail is required. Localisation of the fovea has been proposed by many studies such as found in Sekhar *et al.* [7] who proposed a method for fovea localization based on the spatial relationship with the optic disk and from the spatial distribution of the blood vessels and information of the optic disk has been proposed by Li *et al.* [8]. In this paper, we propose a fast method based on combination of attributes of both aforementioned methods to localise the fovea with better performance.

Information of the retinal blood vessels and the optic disk has significant importance, in our method, to localize the fovea by making use of their geometric relations. Consequently, we followed the method described by Niemeijer *et al.* [9] to localise the optic disk, as shown in Fig 2(c) and the method described by Martenez-Perez *et al.* [10] to detect the main thick blood vessels as shown in Fig. 2(d).

The two main retinal blood vessels, which together are parabolic in shape, have in most retinal images a similar geometric relation with the fovea. Hence, they are fitted as a parabola with a vertex location on the centre of the optic disk. These main vessels are first represented by a number of landmarks and then approximated to a parabola using a Hough transform to map the data into the properly quantised parameter space. But as the number of landmarks is limited and not enough to describe the main courses of the blood vessels, a combination of Hough transform and linear least square fitting techniques was applied, as described in [8].

A candidate region of interest is defined as the part of a sector subtended to the optic disk centre by an angle of  $30^\circ$

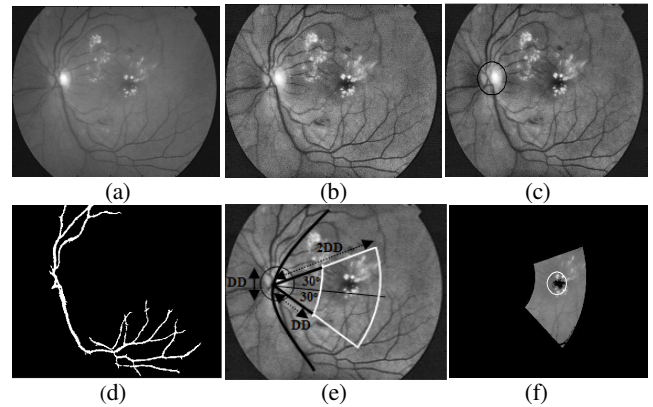


Fig. 2 – Input image and results of pre-processing and fovea localisation steps. (a) A green channel image. (b) A pre-processed image. (c) Image with localised optic disk. (d) Main blood vessels image. (e) Geometry of fovea. (f) Region of interest for locating fovea.

above and below the parabola axis [7]. The angle value is selected so as to circumscribe within the chunk portion a circle of two times the optic disk diameter (DD). Within the selected chunk portion, the threshold value is calculated in such a way that the segmented area is approximately a circle in shape with a diameter of about  $2/3$  of DD [11]. Geometry of the fovea and the chunk portion with a localisation result are illustrated in Fig. 2(e) and Fig. 2(f) respectively.

## 2.3 Detection of Hard Exudates

In retinal images HEs generally appear as bright regions with distinct boundaries. Two operations were carried out to detect HEs: adaptive thresholding and classification. The adaptive thresholding includes two steps: image partitioning into homogeneous regions and then segmenting candidates of HEs from the background of these regions. A classification process was carried out to classify HEs from non-HEs using a rule-based classifier.

### 2.3.1 Adaptive thresholding

Adaptive thresholding is a sophisticated version of thresholding. It takes into account the change of lighting conditions in the image and changes the threshold value over the image. The proposed method aims to perform image segmentation in arbitrary image qualities with better performance and low computational complexity. This method consists of two steps: (1) image partitioning using a technique of top-down image segmentation and (2) HEs segmentation using a combination of edge detection and region growing techniques.

#### A) Top-down image segmentation

It is based on two fundamental steps: image segmentation into smaller regions and region evaluation operations. The process of segmentation should continue until reaching pre-defined criteria to get a number of homogeneous regions, thus being more suitable for accurate HEs detection. In this stage the pre-processed image is used after removing the optic disk to avoid detecting it as exudate. For this, the optic disk location is masked by a disk with a colour equal to the average intensity of the background as shown in Fig 3(a). Procedures of the top-down image segmentation proposed in this method can be summarized as follows:

1. View the entire image as the initial segmentation then describe it by its overall global statistics, namely the mean and the variance.
2. Extract the regions whose local statistics differ considerably from the global statistics.
3. Compute statistics of all the regions extracted in the step 2 to be considered as newly global region statistics.
4. Apply steps 2 and 3 to the new regions until accomplishing the homogeneity for all created regions.

Let  $P$  is a logical predicate used to examine the homogeneity of the region  $R$ . If it is false, the region must be partitioned into several small regions  $R_i$ ,  $i = 1, \dots, n$ , where  $n$  relies on the comparison of local mean values, which are computed inside a small sliding window ( $w \times w$ ), with the global mean value. Otherwise, the region is made permanent. This operation is expressed as follows:

$$R \Rightarrow \begin{cases} \bigcup_{i=1}^n R_i & \text{if } P(R) \text{ is false} \\ R & \text{otherwise} \end{cases}$$

The predicate  $p$  is defined as:

$$P(R) = \begin{cases} \text{true} & \text{if } \max_{(x,y) \in R} [f(x,y)] - \min_{(x,y) \in R} [f(x,y)] \leq \varepsilon \\ \text{false} & \text{otherwise} \end{cases}$$

where  $f(x, y)$  is the gray level of the pixel located at  $(x, y)$  and  $\varepsilon$  is a predefined threshold obtained empirically. Proper selection of  $\varepsilon$  is vital to avoid over or under-segmentation, and to achieve a suitable balance between the performance measures and the time of computation. The trade-off between computational complexity and performance results are also influenced by the sliding window size. Experimental tests showed that a window size of  $w = 15$  turned out as a good compromise between them.

### B) Candidate segmentation

In the absence of any prior knowledge about their presence, sizes, and distribution, HEs cannot be segmented precisely from the entire image with a specific global thresholding method. In the preceding step, the image is subdivided into a number of homogeneous regions to increase the reliability of subsequent HEs detection. To remove contrasted blood vessels from resulting sub-images, a morphological closing operator with disk-shaped structuring element and fixed radius of 6 pixels was used. Then, edges in each region are detected using the Canny edge detector with specifying a scalar sensitivity threshold ( $\alpha$ ) to represent the high threshold for the Canny method and  $0.4\alpha$  is used for the low threshold. For reasonable trade-off between some performance measures particularly sensitivity and positive predictive value (PPV), we carried out edge detection process with  $\alpha = 0.1$ . Second, seeds in each region are selected, then the pixels adjacent to each seed were tested and the regions are allowed to grow until reaching an edge or large gradient. The detection results of HEs candidates in different sub-images were merged to achieve an initial HEs detection image as shown in Fig. 3(b).

### 2.3.2. Classification

To classify HEs and separate them from non- HEs in the initial detection result, two operations were carried out: First a rule-based classifier was used to classify true HEs

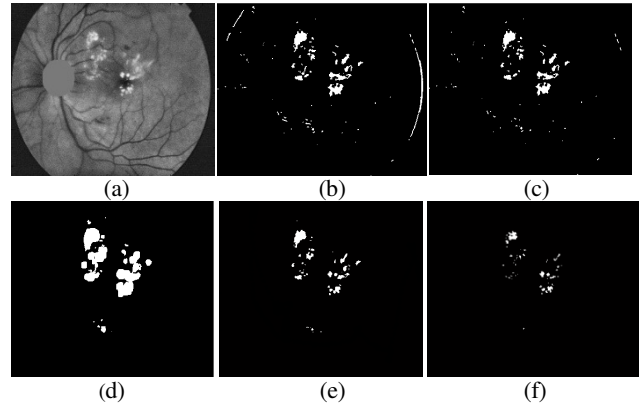


Fig. 3 – Input image and results of exudate detection steps. (a) A green channel image after optic disk removal. (b) A result of top-down segmentation, and HEs candidate segmentation (c) A result of (b) after the first classification step. (d) A result of coarse HEs detection. (e) A result of second classification step (final HEs detection result). (f) A clinician hand-labelled image (ground truth).

from non-HEs based on many features. This system is based on a number of quantities and logical rules. A rule-based classification consists of if-then rules which are used to formulate the conditional statements that comprise the complete knowledge base. Since HEs are lipid leaks from the side of tiny blood vessels, they tend to have spherical shape with diameters greater than feeding blood vessels. However, some exudates are elliptical or slightly elongated, so these slight deviations should be tolerated in the lower limits of the criteria. Consequently, HEs can be discriminated using shape features, such as; length, width, aspect-ratio (ratio of length to width), area, perimeter, circularity (measure of roundness from relation between area and perimeter), solidity and eccentricity. The rules used in this classifier were derived empirically based on many experimental tests. Examples of these rules from specifications of true exudates are: aspect-ratio  $< 1.8$ , circularity  $> 0.5$ , area  $> 25$  and eccentricity  $> 0.75$ . Second, bright objects of distinct boundaries in the pre-processed image are coarsely segmented to highlight only areas which have specifications of HEs. For this, the method described by Jaafar *et al.* [12] was applied. Then the coarse HEs image was combined with the image of the first classification phase using a logical AND operation to reject remaining bright objects which do not have distinct borders (artifacts), to get the final HEs detection image. Resulting images of the first classification phase, coarse HEs image, final HEs image and the ground truth are shown in Fig. 3(c), 3(d), 3(e) and 3(f) respectively.

### 2.4 Grading of Hard Exudates

As the fovea is the centre of vision, the detection of HEs provides more precise and meaningful evaluation of risk when their spatial locations are described with reference to location of the fovea. For this, a fovea coordinate system (FCS) is adopted based on the brief description given by Li *et al.* [8]. Establishment of the FCS is based on the medical polar coordinate system described in [11]. In this system the retina is partitioned into 10 fields where the fovea is their centre as described below and as shown in Fig. 4:

- One central region; called ‘centre’, referred by ‘1’ in Fig. 4 and represented by the innermost circle, centered at detected fovea, of diameter  $2/3$  that of the optic disk (DD).
- Four inner regions; called ‘inner (superior, nasal, inferior and temporal)’, referred by ‘2, 3, 4, 5’ respectively in Fig. 4 and represented by the areas between the circumferences of the innermost circle and the second circle of diameter  $2DD$ .
- Four outer regions; called ‘outer (superior, nasal, inferior and temporal)’, referred by ‘6, 7, 8, 9’ respectively in Fig. 4 and represented by the areas between the circumferences of the second and the outermost circle of diameter  $4DD$ .
- One region; called ‘far temporal’, referred by ‘10’ in Fig. 4, as the area outside the third circle, between 7:30 and 10:30 for the right eyes or between 1:30 and 4:30 for the left eyes.

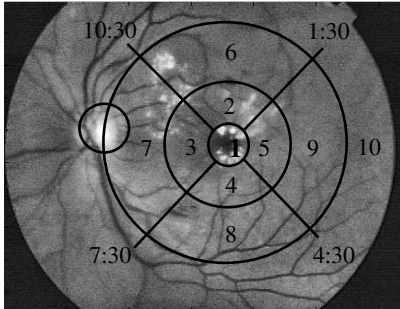


Fig. – 4 An image with FCS overlaid.

### 3. RESULTS AND DISCUSSIONS

We have used a set of 236 retinal images to train and test the proposed method from various databases as follows:

- 130 retinal images of which 110 images contain different signs of DR, according to the evaluation of ophthalmologists, are from DIARETDB0 database [13]. These images are captured at  $50^\circ$  field of view and a size of  $1500 \times 1152$  pixels.
- 89 retinal images of which 47 images contain HEs, according to the evaluation of ophthalmologists are from DIARETDB1 database [14]. These images are captured at  $50^\circ$  field of view and a size of  $1500 \times 1152$  pixels.
- 17 retinal images, all of them contain HEs, are from the Messidor database [6]. These images are captured with a  $45^\circ$  field of view at a size of  $640 \times 480$  pixels. We have selected these 17 images among all images of the Messidor because they are available with their ground truth.

The proposed method was trained and tuned using the set of 130 images and then tested using a set of 106 images (89 from the DIARETDB1 and 17 from the Messidor) where the Messidor images are resized to the size of the DIARETDB1 images. Testing operations were carried out to validate our method with two criteria of resolution: pixel based calculation and image based classification.

Many experiments have been implemented to tune the proposed method after selecting optimal parameter values for the best performance. We assessed the performance of the proposed method with respect to sensitivity, specificity, accuracy and PPV. Performance of the proposed method was assessed quantitatively by comparing its binary results with the clinician hand-labelled data. In pixel based calculation, four types of pixels are considered as follows: true positives

( $TP$ ), false positives ( $FP$ ), false negatives ( $FN$ ), and true negatives ( $TN$ ). These quantities were computed with each individual image to measure the following measures:

$$\begin{aligned} \text{Sensitivity} &= TP / (TP + FN) \\ \text{PPV} &= TP / (TP + FP) \\ \text{Specificity} &= TN / (TN + FP) \\ \text{Accuracy} &= (TP + TN) / (TP + FP + TN + FN) \end{aligned}$$

Overall performance measures achieved by the proposed method were as follows: sensitivity of 93.2%, PPV of 80.7%, specificity of 99.2% and accuracy of 99.4%.

A set of 106 images (from the Messidor and DIARETDB1 databases) was used to test the proposed method in terms of image classification and found to achieve 98.4% sensitivity and 90.5% specificity. With respect to the fovea localization, we achieved a success rate of 100% according to an ophthalmologist’s evaluation.

Robustness of the proposed method could be checked with respect to change of some parameters used in the method. We carried out many experiments to study the influence of the parameters  $\epsilon$  and  $\alpha$  on the performance measures and computation time. It has been found that a manipulation in the threshold  $\epsilon$  has an influence on the balance between performance measures and the computation time as indicated in ROC curve of Fig. 5(a). The sensitivity has been taken here as criterion for the performance because it is the most informative measure. Experimental results showed that increasing of  $\epsilon$  will cause noticeable decrease in the sensitivity and computation time (faster), and vice versa but with slow rate of increase for the sensitivity.

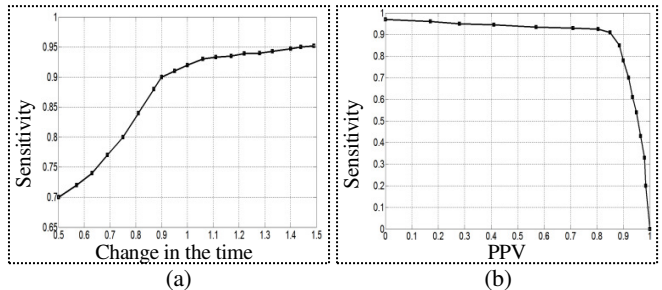


Fig. – 5 ROC curves. (a) Influence of the threshold  $\epsilon$  on the balance between overall sensitivity and the computation time. (b) Influence of the threshold  $\alpha$  on the balance between the sensitivity and PPV.

The manipulation in the threshold  $\alpha$  has an influence on the balance between desired  $TP$  and undesired  $FP$  and as a result on the balance between the sensitivity and the PPV as indicated in the ROC curve of Fig. 5(b). From experimental tests, we observed that changing  $\alpha$  around the selected value will change the balance between the sensitivity and the PPV in a way that an increase in  $\alpha$  will cause decrease in the sensitivity and increase in the PPV and vice versa. We conclude that the behaviour of the proposed method with respect to variation of parameters is robust. Anyhow, the optimal intervention on these parameters relies on the diagnostic requirements and can be decided by the clinician.

To grade detected HEs, they have to be calculated, in terms of pixels, with reference to the FCS fields to be then eva-

luated by specialist based on their sizes and locations. To clarify the importance of HEs grading, two examples are given in Fig. 6. Results of both of them are represented by the white colour on their gray images where the FCS is overlaid. According to [11], HEs in the centre and inner fields affect the vision more than those in the other fields. Consequently, although the HEs in example 1(in (a)) are fewer in both number and size than those in example 2, but they are more harmful on vision and medically more urgent to be treated.

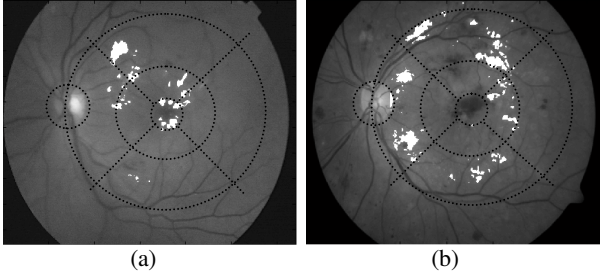


Fig. – 6 Locating of detected HEs with reference to FCS for two examples. (a) Example 1. (b) Example 2.

The training and testing sets used in the proposed method are larger than those used in most previous related works. A comparison of the performance of the proposed method with the other related works, illustrated in Table 1, shows a distinctive sensitivity, in terms of pixels, and superior specificity, in terms of images. As with many works (Garcia *et al.*, Sopharak *et al.*, Walter *et al.* and many others), HEs are detected based on local features such as brightness, sharpness, shapes, area and others. We have used a technique of top-down image segmentation in which the image is dynamically partitioned into homogeneous regions as prerequisite step before HEs segmentation. As a result, the proposed method is characterised by a good ability to deal efficiently with a variety of image quality.

Table – 1 Comparison of performance measures for the proposed method and other previous related works.

Method	Test set	In pixel basis		In image basis	
		SE%	PPV%	SE%	SP%
Osareh [2]	67	93.0	-	95	88.9
Garcia [3]	67	87.6	83.5	100	77.8
Sanchez [4]	80	90.2	96.8	100	90
Sopharak [5]	39	92.3	53.1	-	-
Walter [6]	15	92.8	92.4	100	86.7
Prpsd mthd	106	93.2	80.7	98.4	90.5

Prpsd mthd = proposed method, SE = Sensitivity, SP = Specificity.

#### 4. CONCLUSIONS

In this work, a new decision support framework for automatic detection and grading of HEs has been proposed. In the HEs detection, top-down image segmentation was used to partition the image into homogeneous regions followed by edge detection and region growing to segment HEs candidates before the classification process. A system for HEs grading is presented here, based on two existing works, with more detail clarifications to make it easier for reproducing. The strength of the proposed method is attributed to the

combination of good performance and the ability to deal with a variety of image quality. Although it occasionally fails to get rid of some artifacts, the advantages of the proposed method are believed to be derived from our technique of top-down image segmentation, leading to dynamically partitioned homogeneous image regions. Influence of parameter changes has been studied and the results suggest that the behaviour of the proposed method is quite efficient.

#### 5. ACKNOWLEDGEMENTS

The authors would like to thank the DIARETDB0 Database Centre [13], the DIARETDB1 Database Centre [14] and the Centre of Mathematical Morphology, Mines Paris Tech. [6] for their cooperation in providing retinal images. Hussain F. Jaafar would like to acknowledge the financial support of the Iraqi government.

#### REFERENCES

- [1] D. S. Fong, L. Aiello, T. W. Gardner, G. L. King, G. Blankenship, J. D. Cavallerano, F. L. Ferris and R. Klein, *Diabetic Retinopathy*, Diabetes Care, vol. 26(1), pp. 226-229, 2003
- [2] A. Osareh, M. Mirmehdi, B. Thomas and R. Markham, "Automated identification of diabetic retinal exudates in digital colour images," *British J. of Ophthalmology*, 87, pp. 1220-1223, 2003.
- [3] M. Garcia, C. I. Sanchez, M. I. Lopez, D. Abasolo and R. Hornero, "Neural network basad detección of hard exudates in retinal images," *Computer Methods and Programs in Biomedicine*, vol. 93, pp. 9-19, 2009.
- [4] C. I. Sanchez, M. Garcia, A. Mayo, M. I. Lopez and R. Hornero, "Retinal image analysis based on mixture models to detect hard exudates," *Medical Image Analysis*, vol. 13, pp. 650-658, 2009.
- [5] A. Sopharak, M. N. Dailey, B. Uyyanonvara, B. Sarah, T. Williamson, K. Nwe and Y. Moe, "Machine learning approach to automatic exudate detection in retinal images from diabetic retinopathy," *Journal of Modern Optics*, 57(2), pp. 124-135, 2009.
- [6] T. Walter, J. C. Klein and P. Massin, "A Contribution of image processing to the diagnosis of diabetic retinopathy- detection of exudates in colour fundus images of the human retina," *IEEE Trans. Med. Imaging*, 21, pp. 1236-43, 2002.
- [7] S. Sekhar, W. Al-Nuaimy and A. K. Nandi, "Automated Localization of Optic Disk and Fovea in Retinal Fundus Images," *EUSIPCO 2008*, Switzerland, 2008.
- [8] H. Li and O. Chutatape, "Automated feature extraction in color retinal images by a model based approach," *IEEE Transaction on Medical Engineering*, vol. 51, pp. 246-254, 2004.
- [9] M. Niemeijer, M. D. Abramoff, B. V. Ginneken, "Fast detection of the optic disk and fovea in color fundus photographs," *Medical Image Analysis* 13 pp. 859-870, 2009.
- [10] M. E. Martinez-Perez, et al. , "Segmentation of blood vessels from red-free and fluorescein retinal images," *Medical Image Analysis*, vol. 11, pp. 47-61, 2007.
- [11] ETDRS Report'10, "Grading diabetic retinopathy from stereoscopic color fundus photographs – An extension of the modified Airline house classification," *Ophthalmology*, vol. 98, pp. 786-806, 1991.
- [12] H. F. Jaafar, A. K. Nandi and W. Al-Nuaimy, "Automated detection of exudates in retinal images using a split-and-merge algorithm," *EUSIPCO 2010*, Alborg, pp. 1622-1626, 2010.
- [13] T. Kauppi , *et al.* "DIARETDB0: Evaluation database and morphology for diabetic retinopathy algorithm. Technical report, Lappeenranta University of Technology, Finland, 2006.
- [14] T. Kauppi *et al.* "the DIARETDB1 diabetic retinopathy database and evaluation protocol," Technical report, Lappeenranta University of Tech. and University of Kuopio, Finland, 2007.